Supporting Information

Planavsky et al. 10.1073/pnas.1120387109

SI Text

Global Sulfur Cycle Model. We used a widely employed global sulfur cycle box modeling approach (e.g., 1–3) to explore the dynamics and significance of the carbonate-associated sulfate (CAS) isotope record at the end of the Lomagundi excursion (LE). Gill et al. (2) and Kurtz et al. (4) recently described the modeling approach in detail, so we only provide an overview. We used the following expression to mimic the isotopic change of the global marine sulfate reservoir:

$$\frac{\partial \delta_0}{\partial t} = \frac{F_W(\delta_W - \delta_0) - F_{py}\Delta S}{M_0}$$

where M_0 and δ_0 are the amount of sulfate S in the ocean reservoir and its isotopic composition, respectively. The input to the ocean, F_W, includes sulfur fluxes to the marine system from weathering and magmatic processes, and is assigned a single, average isotopic composition (δw). F_{py} is the pyrite burial flux and ΔS is the mean fractionation from oceanic sulfate caused by bacterial sulfate reduction and pyrite formation. Consistent with the sulfide $\delta^{34}S$ record (e.g., 5), we have used a lower $\Delta^{34}S$ value than is typically used for Phanerozoic modeling work (Fig. S1), and we have assumed a constant $\Delta^{34}S$ throughout the LE. Initial and nonvarying boundary conditions (Fig. S1) are similar to those used in Phanerozoic sulfur cycle models (e.g., 2). The one exception is that evaporate burial, which does not have a significant associated isotopic fractionation, was held below 15% of the modern flux. Estimates of marine sulfur concentrations, along with the reduced to oxidized sulfur ratio of the marine burial flux during the LE are discussed in the main text. We constructed the model using STELLA™ modeling software and employed a forward modeling approach—varying key boundary conditions for the sulfur cycle (Fig. S2), in order to best recreate the observed sulfur isotopic profile.

We have modeled the observed rise in marine sulfate $\delta^{34}S$ values during the falling limb of the LE. More specifically, we modeled a rise in the $\delta^{34}S$ value of marine sulfate from approximately 13‰ to approximately 28‰ over 50 million years (Myr). The observed isotopic shift may have occurred more rapidly than 50 Myr (estimated to have occurred between 30–50 Myr; Fig. 2). However, given that our conclusion is that this isotope shift represents a significant geochemical perturbation, this long timespan is conservative. We suggest the data are best reproduced with a strong (2.7-fold) increase in pyrite burial (relative to the modern global burial flux), a modern continental sulfate flux, a starting marine sulfate concentration of 7 mM, and mean $\Delta^{34}S$ value of −17‰ transiently increasing to −21‰ (Fig. S1). The sulfate $\delta^{34}S$ values can also be reproduced with an elevated continental sulfate flux. However, with a larger continental sulfate flux, an increase in the global pyrite burial flux is needed to reproduce the rise in $\delta^{34}S$ values at the tail end of the LE. For instance, a 3.2-fold increase in the global pyrite burial flux relative to the modern is needed given a transient decrease from 115% to 100% of the modern continental sulfate flux over the 50-Myr period. Model runs using very elevated continental sulfate fluxes ($\gtrsim$ 120% of the modern flux), without inducing extensive gypsum burial (at least 50% modern evaporate burial), yield very high (>20 mM) marine sulfate concentrations. Marine sulfate concentrations above 20 mM are inconsistent with available estimates for the size of the marine sulfate reservoir in the mid-Paleoproterozoic (see main text).

Sensitivity tests for key model variables are shown in Fig. S2. The model is sensitive enough to pyrite burial (Fig. S2*A*) that the percent increase in pyrite burial can be estimated within a relatively narrow range (an increase in pyrite burial to >2.15 and <3.15 times the modern flux). However, as noted above, if the observed rise in carbonate-associated sulfate (CAS) $\delta^{34}S$ values occurred over a shorter time period than estimated, larger increases in pyrite burial will be needed (Fig. S2*A*). The model is also very sensitive to the magnitude of the continental weathering flux (all other parameters being held constant)—15% changes in the magnitude of the continental sulfate flux lead to large (>5 mM) changes in the peak marine sulfate concentrations (Fig. S2*B*). The starting sulfate concentration makes little difference on the trajectory of the isotopic profile (Fig. S2*C*), but does affect the peak sulfate concentration and the sulfate concentration at the end of the event. In contrast, strong (>10‰) shifts in the ΔS value can significantly decrease (>10 Myr) the time needed to induce the observed isotopic shift, but varying the ΔS value has no effect on the sulfate concentrations (Fig. S2*D*). However, there is not current evidence that global mean pyrite $\delta^{34}S$ values varied substantially throughout the mid-Paleoproterozoic (e.g., 5).

It has been proposed that an increase in hydrothermal activity can cause an antithetic relationship in marine sulfate $\delta^{34}S$ and carbonate $\delta^{13}C$ records, with light $\delta^{34}S$ values being linked to strong mantle-derived sulfur fluxes (6, 7). Although the end of the Lomagundi excursion coincides with the breakup of Kenorland and, likely, enhanced hydrothermal activity, we note that the pattern predicted by this model is opposite from what we observe in the rock record (Fig. 2). A shift to positive carbon isotope values is expected with enhanced hydrothermal activity and downward trend in S isotope values (6, 7). Given this framework, any changes in the hydrothermal S flux during the LE would require more pronounced shifts in pyrite burial at the end of the LE than we have predicted. We have not varied the hydrothermal sulfur flux in the model runs, which renders our conclusions conservative.

1. Garrels RM, Lerman A (1984) Coupling of the sedimentary sulfur and carbon cycles: An improved model. *Am J Sci* 284:989–1007.
2. Gill BC, et al. (2011) Geochemical evidence for widespread euxinia in the Later Cambrian ocean. *Nature* 469:80–83.
3. Kump LR, Garrels RM (1986) Modeling atmospheric O2 in the global sedimentary redox cycle. *Am J Sci* 286:337–360.
4. Kurtz AC, Kump LR, Arthur MA, Zachos JC, Paytan A (2003) Early Cenozoic decoupling of the global carbon and sulfur cycles. *Palaeogeogr Palaeoclimatol Palaeoecol*, 10 .1029/2003PA000908.
5. Canfield DE (2004) The evolution of the Earth surface sulfur reservoir. *Am J Sci* 304:839–861.
6. Carpenter SJ, Lohmann KC (1997) Carbon isotope ratios of Phanerozoic marine cements: Re-evaluating the global carbon and sulfur systems. *Geochim Cosmochim Acta* 61:4831–4846.
7. Walker JCG (1986) Global geochemical cycles of carbon, sulfur and oxygen. *Mar Geol* 70:159–174.

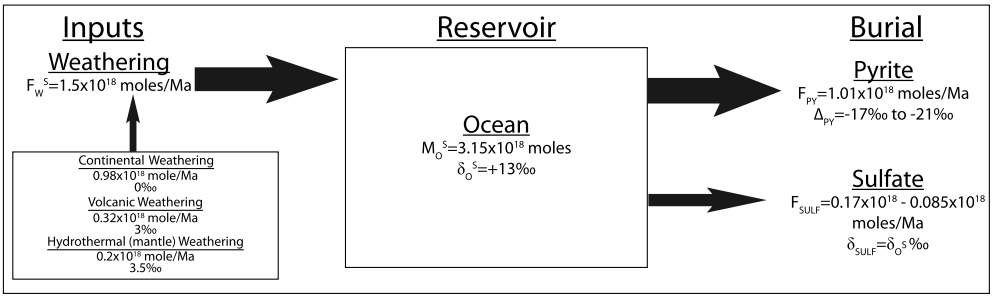

Fig. S1. Overview of utilized global sulfur cycle model parameters.

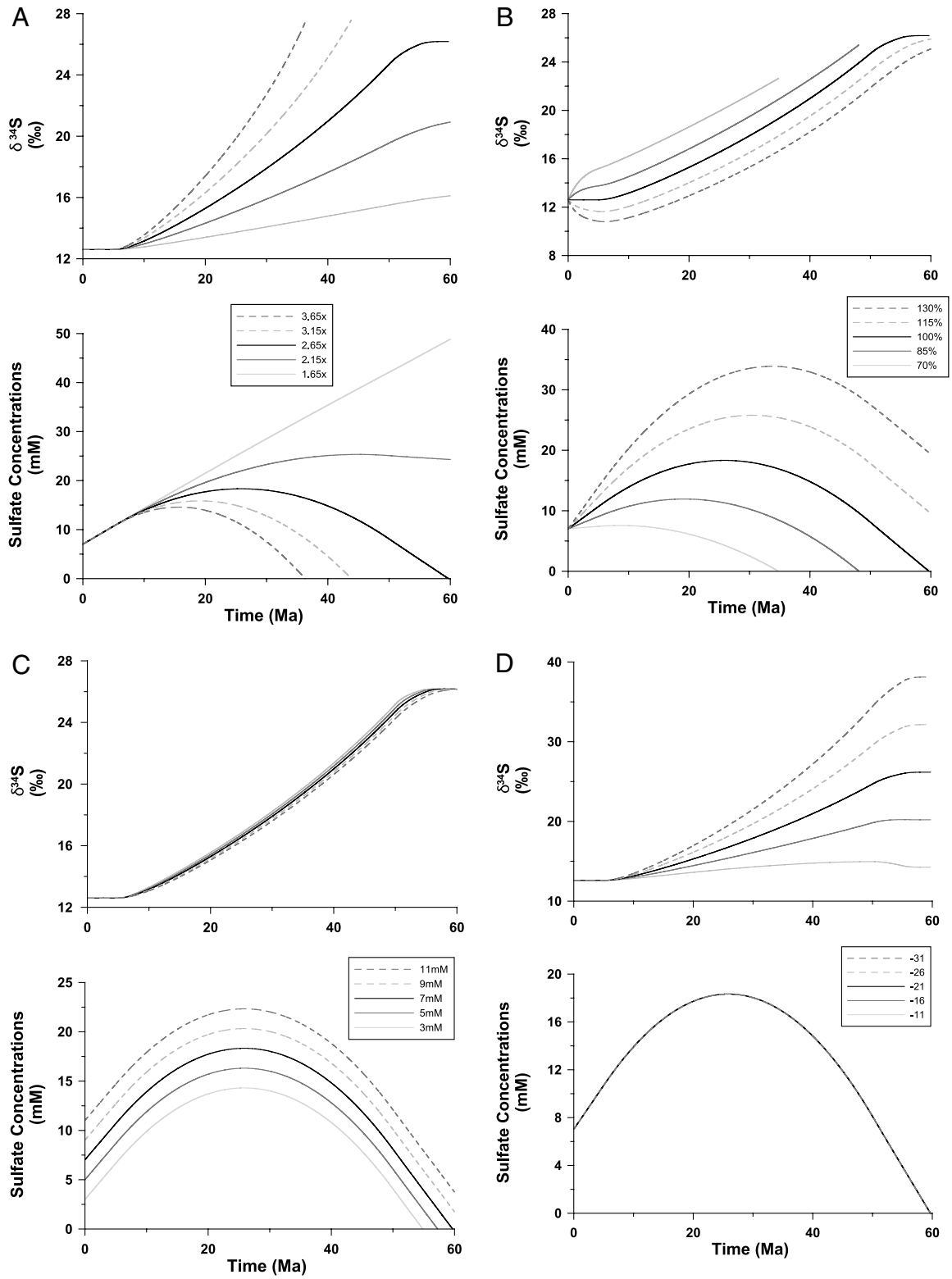

Fig. S2. Sensitivity tests for global S cycle model. We modeled a rise in the $\delta^{34}S$ value of marine sulfate from approximately 13‰ to approximately 28‰ over 50 Myr during the end of the Lomagundi excursion. We suggest the data are best reproduced with a 2.7-fold increase in pyrite burial relative to the global modern burial flux, a modern continental sulfate flux, a starting marine sulfate concentration of 7 mM, and mean $\Delta^{34}S$ value of −17‰ transiently increasing to −21‰. All sensitivity tests (*A*–*D*) use these model parameters. (*A*) Effects of variations in the magnitude of the pyrite burial flux on the trajectory of the $\delta^{34}S$ value rise and on the size of the global marine sulfate reservoir. (*B*) Effects of variations in the magnitude of the continental weathering (sulfate) flux on the trajectory of the $\delta^{34}S$ value rise and on the size of the global marine sulfate reservoir. (*C*) Effects of variations in initial marine sulfate concentrations on the trajectory of the $\delta^{34}S$ value rise and on the size of the global marine sulfate reservoir. (*D*) Effects of variations in pyrite fractionation factors ($\Delta^{34}S$ values) on trajectory of the $\delta^{34}S$ value rise and on the size of the global marine sulfate reservoir.

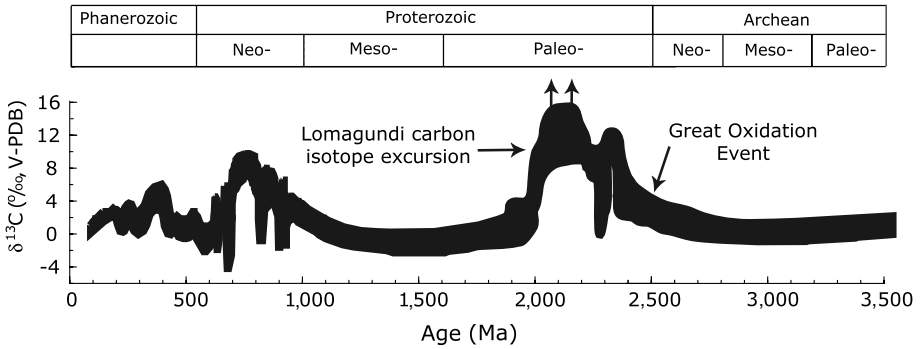

Fig. S3. Generalized carbonate-carbon isotope curve through time. The Lomagundi positive carbon isotope excursion is the longest and largest deviation from the near-zero $\delta^{13}C$ values typical of carbonates throughout Earth's history. The onset of the Lomagundi excursion closely follows the initial rise in atmospheric oxygen (cf. 1). Based on the global pattern of carbon isotope values in Paleoproterozoic marine carbonates, the Lomagundi excursion likely encompassed at least two separate intervals of markedly positive $\delta^{13}C$ values. Modified from ref. 2.

1 Bekker A, et al. (2004) Dating the rise of atmospheric oxygen. *Nature* 427:117.
2 Karhu JA (1999) *Encyclopedia of Geochemistry,* eds Marshall CP, Fairbridge RW (Kluwer Academic Publishers, Boston), pp 67–73.

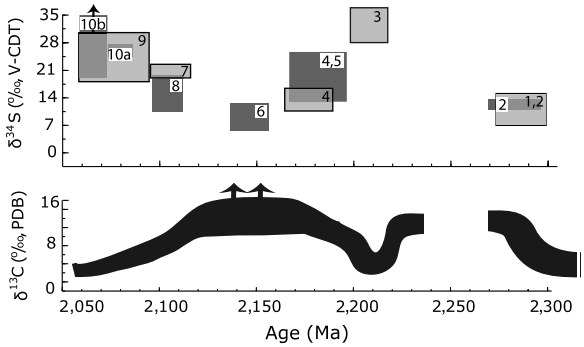

Fig. S4. A generalized $\delta^{13}C_{carbonate}$ trend and available sulfate $\delta^{34}S$ values for the *ca*. 2.3–2.05-billion-year (Ga) time interval. Light-grey boxes are $\delta^{34}S$ values for sulfate evaporite (gypsum and anhydrite), and dark-grey boxes are $\delta^{34}S_{CAS}$ data from this study. The $\delta^{13}C_{carbonate}$ curve is modified from ref. 1, and the compilation of sulfate evaporite S isotope values is from ref. 2 (also presented in Table S4). The $\delta^{34}S_{CAS}$ values are from this study. The ages of the units (and the duration) is based on the available constraints from radiometric ages (see ref. 2) and the carbonate-carbon isotope data, relative to the idealized carbon isotope curve. 1, Gordon Lake Formation; 2, Kona Dolomite; 3, Lower Umba Formation; 4, Lucknow Formation; 5, Silverton Formation; 6, Nash Fork; 7, Delwara Formation and Jhamarkotra Formation; 8, Mcheka Formation; 9, Fedorovka Formation; 10a, Lower Albanel Formation (Lomagundi Excursion); 10b, Lower Albanel Formation (post Lomagundi Excursion)

1 Bekker A, Karhu JA, Kaufman AJ (2006) Carbon isotope record for the onset of the Lomagundi carbon isotope excursion in the Great Lakes area, North America. *Precambrian Res* 148:145–180.
2 Schröeder S, Bekker A, Beukes NJ, Strauss H, van Niekerk HS (2008) Rise in seawater sulphate concentration associated with the Paleoproterozoic positive carbon isotope excursion: Evidence from sulphate evaporites in the similar to 2.2–2.1 Gyr shallow-marine Lucknow Formation, South Africa. *Terra Nova* 2:108–117.

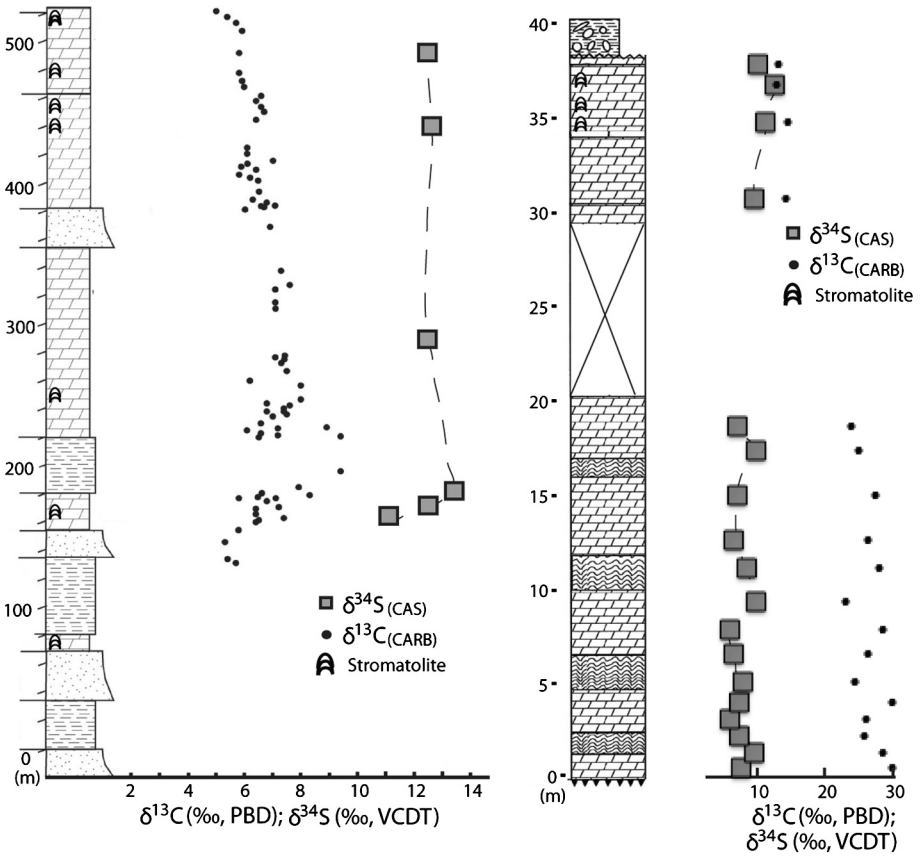

Fig. S5. Carbonate $\delta^{13}C$ and $\delta^{34}S_{CAS}$ stratigraphic trends in the (*A*) Kona Dolomite, United States (modified from ref. 1), and (*B*) Nash Fork Formation, United States (modified from ref. 2).

1 Bekker A, Karhu JA, Kaufman AJ (2006) Carbon isotope record for the onset of the Lomagundi carbon isotope excursion in the Great Lakes area, North America. *Precambrian Res* 148:145–180.

2 Bekker A, Karhu JA, Eriksson KA, Kaufman AJ (2003) Chemostratigraphy of Paleoproterozoic carbonate successions of the Wyoming Craton: Tectonic forcing of biogeochemical change? *Precambrian Res* 120:279–325.

Table S1. Sulfur and carbon data for examined Paleoproterozoic carbonates

Formation/member	Sample name	$\delta^{34}S$ CAS	[CAS]	$\delta^{13}C$ carbonate	$\delta^{18}O$ carbonate	Timing within the LE	Reference on basic geology and correlation
Espanola	EL-2	21.6				Preceding	Bekker et al. (1)
Espanola	El-4	19.7				Preceding	Bekker et al. (1)
Espanola	EL-11	20.3		−2.0	−16.0	Preceding	Bekker et al. (1)
Espanola	EL-34	17.9		−2.0	−14.8	Preceding	Bekker et al. (1)
Espanola	EL-35A	15.0		−2.0	−15.4	Preceding	Bekker et al. (1)
Espanola	EL-39	21.0		−2.1	−13.7	Preceding	Bekker et al. (1)
Espanola	EL-56	29.1		−1.9	−15.7	Preceding	Bekker et al. (1)
Espanola	El-THR-3	15.7				Preceding	Bekker et al. (1)
Kona	MM-30	11.2	121	6.4	−12.4	Early	Bekker et al. (2)
Kona	MM-33	12.7	146	6.4	−12.4	Early	Bekker et al. (2)
Kona	MM-35	13.9		6.4	−11.8	Early	Bekker et al. (2)
Kona	MM-56	12.7		7.1	−12.9	Early	Bekker et al. (2)
Kona	MM-81	12.8		6	−12	Early	Bekker et al. (2
Kona	MM-90	12.7		5.4	−10.9	Early	Bekker et al. (2)
Silverton	Si-5B	12.5	95	9.8	−6.8	Middle	Bekker et al. (3)
Silverton	Si-5A	13.1	70	8.7	−7.9	Middle	Bekker et al. (3)
Silverton	SI-3	13.6	86	9.8	−13.2	Middle	Bekker et al. (3)
Silverton	SI-2/8	14.0		9.74	−8.6	Middle	Bekker et al. (3)
Silverton	SI-2/7	14.9		10.0	−7.0	Middle	Bekker et al. (3)
Silverton	SI-2/14	14.0		10.3	−9.4	Middle	Bekker et al. (3)
Silverton	SI-2-6	11.3		9.4	−9.4	Middle	Bekker et al. (3)
Silverton	Si-2-13	16.0		9.8	−13.2	Middle	Bekker et al. (3)
Lucknow	LK-1	25.8		10.3	−6.7	Middle	Bekker et al. (4); Schröder et al. (5)
Lucknow	LK-2	12.8	274	9.4	−8.0	Middle	Bekker et al. (4); Schröder et al. (5)
Lucknow	LK-3	23.4		10.0	−7.5	Middle	Bekker et al. (4); Schröder et al. (5)
Lucknow	LK-4	26.0		9.7	−6.5	Middle	Bekker et al. (4); Schröder et al. (5)

Formation/member	Sample name	δ^{34}S CAS	[CAS]	δ^{13}C carbonate	δ^{18}O carbonate	Timing within the LE	Reference on basic geology and correlation
Lucknow	LK-9	12.7	393	8.8	−7.4	Middle	Bekker et al. (4); Schröder et al. (5)
Lucknow	Lk-13	25.3	77	10.0	−6.9	Middle	Bekker et al. (4); Schröder et al. (5)
Lucknow	Lk-14	24.5	165	9.5	−6.6	Middle	Bekker et al. (4); Schröder et al. (5)
Nash Fork	BM-1	7.4	151	29.5	−9.2	Middle	Bekker et al. (6)
Nash Fork	BM-2	9.3		28.2	−11.0	Middle	Bekker et al. (6)
Nash Fork	BM-3	6.9	153	25.4	−11.9	Middle	Bekker et al. (6)
Nash Fork	BM-4	5.7	46	25.6	−12.3	Middle	Bekker et al. (6)
Nash Fork	BM-5	7.1	61	29.6	−9.7	Middle	Bekker et al. (6)
Nash Fork	BM-6	7.4	129	24.0	−12.8	Middle	Bekker et al. (6)
Nash Fork	BM-7	6.3	356	25.9	−11.2	Middle	Bekker et al. (6)
Nash Fork	BM-8	5.6		28.1	−9.5	Middle	Bekker et al. (6)
Nash Fork	BM-9	9.6	37	22.7	−10.5	Middle	Bekker et al. (6)
Nash Fork	BM-10	8.2	340	27.5	−10.5	Middle	Bekker et al. (6)
Nash Fork	BM-11	6.2	78	25.9	−11.5	Middle	Bekker et al. (6)
Nash Fork	BM-12	6.8	80	27.1	−10.7	Middle	Bekker et al. (6)
Nash Fork	BM-13	9.5	376	24.7	−11.2	Middle	Bekker et al. (6)
Nash Fork	BM-14	6.8	698	23.5	−11.7	Middle	Bekker et al. (6)
Nash Fork	BM-15	9.1	150	13.9	−10.4	Middle	Bekker et al. (6)
Nash Fork	BM-16	11.0	191	14.3	−12.2	Middle	Bekker et al. (6)
Nash Fork	BM-17	12.2	612	12.6	−13.8	Middle	Bekker et al. (6)
Nash Fork	BM-18	9.7	251	12.9	−13.7	Middle	Bekker et al. (6)
Mcheka	ZA-1	9.5	132	11.1	−6.9	Middle-late	Master et al. (7)
Mcheka	ZA-2	10.2		11.9	−4.6	Middle-late	Master et al. (7)
Mcheka	ZA-3	9.8	111	12.3	−5.6	Middle-late	Master et al. (7)
Mcheka	ZA-4	10.0		11.3	−5.6	Middle-late	Master et al. (7)
Mcheka	ZA-6	11.1	209	11.8	−5.0	Middle-late	Master et al. (7)
Mcheka	ZA-7	11.3	69	10.4	−5.7	Middle-late	Master et al. (7)
Mcheka	ZA-8	11.1	65	11.1	−5.0	Middle-late	Master et al. (7)
Mcheka	ZA-9	11.1	110	11.2	−3.9	Middle-late	Master et al. (7)
Mcheka	ZA-10	11.2	266	11.0	−4.9	Middle-late	Master et al. (7)
Mcheka	ZA-11	11.0	396	11.0	−5.2	Middle-late	Master et al. (7)
Mcheka	ZA-12	10.5	80	10.1	−5.9	Middle-late	Master et al. (7)
Mcheka	ZA-13	10.5	55	10.5	−5.6	Middle-late	Master et al. (7)
Mcheka	ZA-16	11.0	192	10.3	−5.3	Middle-late	Master et al. (7)
Mcheka	ZA-18	11.3	44	9.5	−6.4	Middle-late	Master et al. (7)
Mcheka	ZA-19	10.5	162	10.3	−5.1	Middle-late	Master et al. (7)
Mcheka	ZA-20	13.2	49	10.6	−4.4	Middle-late	Master et al. (7)
Mcheka	ZA-22	12.0	77	10.0	−5.8	Middle-late	Master et al. (7)
Mcheka	ZA-26	11.8	13	9.5	−7.1	Middle-late	Master et al. (7)
Mcheka	ZA-27	11.9	109	10.1	−5.2	Middle-late	Master et al. (7)
Mcheka	ZA-30	14.0	56	9.1	−5.6	Middle-late	Master et al. (7)
Mcheka	ZA-31	16.8	187	9.0	−6.6	Middle-late	Master et al. (7)
Mcheka	ZA-33	12.3	163	8.6	−6.3	Middle-late	Master et al. (7)
Mcheka	ZA-35	12.8	422	8.5	−5.9	Middle-late	Master et al. (7)
Mcheka	ZA-35-2	12.7		8.5	−6.6	Middle-late	Master et al. (7)
Mcheka	ZA-37	15.1	133	8.3	−6.1	Middle-late	Master et al. (7)
Mcheka	Z-3	16.0	49	8.0	−6.5	Middle-late	Master et al. (7)
Mcheka	Z-8	19.1	41	8.1	−5.6	Middle-late	Master et al. (7)
Mcheka	Z-11	15.0	31	8.1	−6.2	Middle-late	Master et al. (7)
Mcheka	Z-13	14.0		7.9	−7.3	Middle-late	Master et al. (7)
Mcheka	Z-15	13.1		8.1	−6.7	Middle-late	Master et al. (7)
Mcheka	Z-16	17.8	31	7.9	−6.6	Middle-late	Master et al. (7)
Mcheka	Z-19	17.8		8.0	−6.8	Middle-late	Master et al. (7)
Mcheka	Z-2	16.3	33	7.8	−6.6	Middle-late	Master et al. (7)
Mcheka	Z-20	19.0		7.9	−6.8	Middle-late	Master et al. (7)
Mcheka	Z-21	16.7	27	8.3	−5.8	Middle-late	Master et al. (7)
Mcheka	Z-25	17.6	28	7.6	−7.3	Middle-late	Master et al. (7)
Mcheka	Z-26	13.7	16	7.7	−6.7	Middle-late	Master et al. (7)
Mcheka	SLD-9	14.6		9.5	−7.6	Middle-late	Master et al. (7)
Mcheka	SLD-14-1	9.4		11.1	−6.3	Middle-late	Master et al. (7)
Mcheka	SLD-14-2	9.4	302	11.1	−6.3	Middle-late	Master et al. (7)
Mcheka	SLD-15	8.2		11.8	−6.1	Middle-late	Master et al. (7)
Mcheka	SLD-20	8.8		11.4	−6	Middle-late	Master et al. (7)
Mcheka	SLD-21	9.3		11.8	−5.9	Middle-late	Master et al. (7)
Mcheka	SLD-24	12.4		11.7	−4.7	Middle-late	Master et al. (7)
Mcheka	SLD-28	12.6		10.9	−5.7	Middle-late	Master et al. (7)
Mcheka	SLD-32	10.8		10.6	−5.2	Middle-late	Master et al. (7)
Mcheka	SLD-35	12.9		9.6	−6.7	Middle-late	Master et al. (7)
Mcheka	SLD-38	12.1		10.0	−5.3	Middle-late	Master et al. (7)
Mcheka	NJ-6	16.6		7.1	−9.9	Middle-late	Master et al. (7)
Lower Albanel	MI-18-2	27.7	32	4.8	−8.5	Late	Bekker et al. (6)

Formation/member	Sample name	δ^{34}S CAS	[CAS]	δ^{13}C carbonate	δ^{18}O carbonate	Timing within the LE	Reference on basic geology and correlation
Lower Albanel	MI-16-5	30.9		5.4	−7.9	Late	Bekker et al. (6)
Lower Albanel	MI-16-2	28.3		5.3	−8.7	Late	Bekker et al. (6)
Lower Albanel	MI-14-66	28.8				Late	Bekker et al. (6)
Lower Albanel	MI-18-4	19.4		1.0	−8.1	Post	Bekker et al. (6)
Lower Albanel	LA-2	18.1	29	1.1	−4.9	Post	Bekker et al. (6)
Lower Albanel	LAF-F3	46.6	37	1.5	−4.4	Post	Bekker et al. (6)
Lower Albanel	UAF-2		42	2.1	−6.5	Post	Bekker et al. (6)
Lower Albanel	UAF-1	42.0	52	2.2	−6.5	Post	Bekker et al. (6)
Lower Albanel	LA-E4	37.1	39	1.1	−3.0	Post	Bekker et al. (6)
Lower Albanel	LAF-4	43.0	66	−0.9	−11.0	Post	Bekker et al. (6)
Lower Albanel	LA-D5	30.1	48	2.4	−3.4	Post	Bekker et al. (6)
Lower Albanel	LAF-D2	31.3	67	2.8	−3.2	Post	Bekker et al. (6)

1 Bekker A, Kaufman AJ, Karhu JA, Eriksson KA (2005) Evidence for Paleoproterozoic cap carbonates in North America. *Precambrian Res* 137:167–206.
2 Bekker A, Karhu JA, Kaufman AJ (2006) Carbon isotope record for the onset of the Lomagundi carbon isotope excursion in the Great Lakes area. *Precambrian Res* 148:145–180.
3 Bekker A, et al. (2008) Fractionation between inorganic and organic carbon during the Lomagundi (2.22–2.1 Ga) carbon isotope excursion. *Earth Planet Sci Lett* 271:278–291.
4 Bekker A, et al. (2001) Chemostratigraphy of the Paleoproterozoic Duitschland Formation, South Africa: Implications for coupled climate change and carbon cycling. *Am J Sci* 301:261–285.
5 Schröder S, Bekker A, Beukes NJ, Strauss H, vanNiekerk HS (2008) Rise in seawater sulphate concentration associated with the Paleoproterozoic positive carbon isotope excursion: Evidence from sulphate evaporites in the similar to 2.2–2.1 Gyr shallow-marine Lucknow Formation, South Africa. *Terra Nova* 20:108–117.
6 Bekker A, Eriksson KA (2003) A Paleoproterozoic drowned carbonate platform on the southeastern margin of the Wyoming Craton: A record of the Kenorland breakup. *Precambrian Res* 120: 327–364.
7 Master S, Bekker A, Hofmann A (2010) A review of the stratigraphy and geological setting of the Palaeoproterozoic Magondi Supergroup, Zimbabwe–Type locality for the Lomagundi carbon isotope excursion. *Precambrian Res* 182:254–273.
8 Bekker A, Karhu JA, Eriksson KA, Kaufman AJ (2003) Chemostratigraphy of Paleoproterozoic carbonate successions of the Wyoming Craton: Tectonic forcing of biogeochemical change? *Precambrian Res* 120: 279–325.

Table S2. Proterozoic and Paleozoic CAS concentrations

Age	Average [CAS] (ppm)	1σ (ppm)	Location	Reference
Late Cambrian	299	164	North Australia, central USA	Gill et al. (1)
Mid-Neoproterozoic	65	66	South Australia, Namibia, southwestern USA	Hurtgen et al. (2)
Mid-Mesoproterozoic, late Paleoproterozoic	20	9	North Australia, central USA	Gellatly et al. (3)
Mid-Mesoproterozoic, late Paleoproterozoic	143	100	North China	Chu et al. (4)
Mid-Paleoproterozoic, (final stages and the aftermath of the LE)	48	12	Mistassini Basin, eastern Canada	This study
Mid-Paleoproterozoic, (middle to end of the LE)	117	110	Upper part of Mcheka Formation, Zimbabwe	This study
Mid-Paleoproterozoic (middle part of the LE)	227	137	Lucknow Formation, South Africa	This study
Mid-Paleoproterozoic, (middle part of the LE)	232	198	Nash Fork Formation, western USA	This study
Early to mid-Paleoproterozoic (all)	150	145	Central and western USA, Zimbabwe, eastern Canada, South Africa	This study

1 Gill BC, et al. (2011) Geochemical evidence for widespread euxinia in the Later Cambrian ocean. *Nature* 469:80–83.
2 Hurtgen MT, Arthur MA, Halverson GP (2005) Neoproterozoic sulfur isotopes, the evolution of microbial sulfur species, and the burial efficiency of sulfide as sedimentary pyrite. *Geology* 33:41–44.
3 Gellatly AM, Lyons TW (2005) Trace sulfate in mid-Proterozoic carbonates and the sulfur isotope record of biospheric evolution. *Geochim Cosmochim Acta* 69:3813–3829.
4 Chu XL, Zhang TG, Zhang QR, Lyons TW (2007) Sulfur and carbon isotope records from 1700 to 800 Ma carbonates of the Jixian section, northern China: Implications for secular isotope variations in Proterozoic seawater and relationships to global supercontinental events. *Geochim Cosmochim Acta* 71:4668–4692.

Table S3. Estimates of marine sulfate concentrations through time

Eon/era	Age (Myr)	Estimate of marine [sulfate] (mM)	Basis for estimate	Reference
Phanerozoic	542–0	*ca*. 5–30	Direct measurement of [sulfate] from fluid inclusions	Lowenstein et al. (1); Horita et al. (2); Brennan et al. (3)
Paleozoic	542–251	*ca*. 5–30	Extent of CAS isotopic variability during positive carbon isotope excursions	Gill et al. (4)
Proterozoic	1,650–630	*ca*. 1–7	Extent of CAS isotopic variability in thick carbonate successions	Kah et al. (5)
Proterozoic	2,100; 1,300; 1,200; 800	>2.5	Presence of thick sulfate evaporate successions and precipitation of sulfate before halite during the evaporation sequences	Schröder et al. (6)
Paleoproterozoic	2,100; 2,250	*ca*. 5–20	Extent of CAS isotopic variability during the falling limb of the Lomagundi positive carbon isotope excursion	This study

Eon/era	Age (Myr)	Estimate of marine [sulfate] (mM)	Basis for estimate	Reference
Mid-Proterozoic	18,00–700	<1	Maximum sulfur isotope fractionation during bacterial sulfate reduction based on the temporal isotopic record of pyrite and sulfate	Canfield et al. (7)
Archean	3,800–2,500	<0.2	Maximum sulfur isotope fractionation during bacterial sulfate reduction based on the temporal isotopic record of pyrite and sulfate	Habicht et al. (8)

1 Lowenstein TK, Timofeeff MN, Brennan ST, Hardie LA, Demicco RV (2001) Oscillations in Phanerozoic seawater chemistry: Evidence from fluid inclusions. *Science* 294:1086–1088.
2 Horita J, Zimmermann H, Holland HD (2002) Chemical evolution of seawater during the Phanerozoic: Implications from the record of marine evaporites. *Geochim Cosmochim Acta* 66:3733–3756.
3 Brennan ST, Lowenstein TK, Horita J (2004) Seawater chemistry and the advent of biocalcification. *Geology* 32:473–476.
4 Gill BC, Lyons TW, Saltzman MR (2007) Parallel, high-resolution carbon and sulfur isotope records of the evolving Paleozoic marine sulfur reservoir. *Palaeogeogr Palaeoclimatol Palaeoecol* 256:156–173.
5 Kah LC, Lyons TW, Frank T (2004) Low marine sulphate and protracted oxygenation of the Proterozoic biosphere. *Nature* 431:834–837.
6 Schröder S, Bekker A, Beukes NJ, Strauss H, van Niekerk HS (2008) Rise in seawater sulphate concentration associated with the Paleoproterozoic positive carbon isotope excursion: Evidence from sulphate evaporites in the similar to 2.2–2.1 Gyr shallow-marine Lucknow Formation, South Africa. *Terra Nova* 20:108–117.
7 Canfield DE, Farquhar J, Zerkle AL (2010) High isotope fractionations during sulfate reduction in a low-sulfate euxinic ocean analog. *Geology* 38:415–418.
8 Habicht KS, Gade M, Thamdrup B, Berg P, Canfield DE (2002) Calibration of sulfate levels in the Archean Ocean. *Science* 298:2372–2374.

Table S4. Sulfur isotope data from evaporites deposited during the Lomagundi excursion

Name of unit (location)	Age (Ga)	Type of evaporite	$\delta^{13}C$ (‰)	$\delta^{34}S$ (‰)	Reference
Gordon Lake Formation, Huronian Supergroup (Lake Huron, Canada)	*ca*. 2.3–2.22	Silicified and pristine anhydrite and gypsum nodules and layers	5.0–8.2	11.7–15.6	Cameron (1), Chandler (2), Bennett et al. (3), Bekker et al. (4)
Kona Dolomite, Chocolay Group (Michigan, USA)	*ca*. 2.3–2.22	Pseudomorphs after gypsum and anhydrite	5.0–9.5	11.4–16.0	Bekker et al. (4), Taylor (5), Clark (6), Wohlabaugh (7), Hemzacek et al. (8), Hemzacek (9), Perry et al. (10), Feng (11), Genest (12)
Lower Umba Formation, Lower Jatulian Group (Imandra–Varzuga Belt, Kola Peninsula, Russia)	*ca*. 2.2	Barite beds	2.3–6.7	27.8–34.2	Melezhik and Fetisova (13), Grinenko et al. (14), Melezhik and Fallick (15)
Lucknow Formation, Postmasburg Group (South Africa)	*ca*. 2.15	Molds and quartz pseudomorphs after gypsum and anhydrite	8.4–11.3	9.2–14.0	Master et al. (16), Swart (17), Schröder et al. (18)
Delwara Formation and Jhamarkotra Formation, Aravalli Group (Rajasthan, India)	*ca*. 2.1	Barite layers	5.1–11.1	17.1–21.2	Deb et al. (19), Sreenivas et al. (20)
Fedorovka Formation (Aldan Shield, Siberia, Russia)	*ca*. 2.1	Anhydrite layers and veins	−1.7–5.5	up to 32.1	Zolotarev et al. (21), Velikoslavinsky et al. (22), Guliy and Wada (23)

Table after Bekker et al. (4) and Schröder et al. (16).

1 Cameron EM (1983) Evidence from early Proterozoic anhydrite for sulfur isotopic partitioning in Precambrian oceans. *Nature* 304:54–56.
2 Chandler FW (1988) Diagenesis of sabkha related, sulphate nodules in the Early Proterozoic Gordon Lake Formation, Ontario, Canada. *Carbonates Evaporites* 3:75–94.
3 Bennett G, Born P, Hatfield K (1989) A report on a recently identified dolostone unit in Fenwick Township, Goulais Bay area, District of Algoma. *Ont Geol Surv Misc Pap* 142:211–215.
4 Bekker A, Karhu JA, Kaufman AJ (2006) Carbon isotope record for the onset of the Lomagundi carbon isotope excursion in the Great Lakes area, North America. *Precambrian Res* 148:145–180.
5 Taylor GL (1972) Stratigraphy, sedimentology, and sulfide mineralization of the Kona Dolomite. PhD dissertation (Michigan Technological Institute, Lansing, MI).
6 Clark JL (1974) Sulfide mineralization in the Kona Dolomite, Marquette County, Michigan. Master's thesis (Michigan Technological University, Houghton, MI).
7 Wohlabaugh N (1980) *Petrology of the Big Cusp Algal Dolomite; An Informal Member of the Kona Dolomite*. (Michigan Bowling Green State University, Marquette).
8 Hemzacek JM, Perry EC, Larue DK, Feng J (1982) Sulfur isotope composition of sulfate in chert horizons of the Proterozoic (Precambrian X) Kona Dolomite, Marquette Region, Michigan. *Geol Soc Am Abstr* 14:512.
9 Hemzacek JM (1987) Replaced evaporites and the sulfur isotope age curve of the Precambrian. Master's thesis (Northern Illinois University, DeKalb, IL).
10 Perry EC, Feng J, Hemzacek JM (1984) Precambrian evaporites: Preservation of sulfate in quartz pseudomorphs after gypsum. *Proc Inst Lake Superior Geol* 30:47.
11 Feng J (1986) Sulfur and oxygen isotope geochemistry of Precambrian marine sulfate and chert. Master's thesis (Northern Illinois University, DeKalb, IL).
12 Genest S (1985) Aphebian evaporites and related red beds in the Peribonca Formation (Otish Group, Central Quebec): Evidence for coastal sabkha and subaqueous environments. *GAC-MAC Programs Abstr* 10:A21.
13 Melezhik VA, Fetisova OA (1989) First discovery of syngenetic barites in the Precambrian of the Baltic Shield. *Doklady Akademii Nauk* 307:422–425.
14 Grinenko LN, Melezhik VA, Fetisova OA (1989) First discovery of barites in the Precambrian sedimentary deposits of Baltic Shield. *Dokl Akad Nauk* 304:1453–1455.
15 Melezhik VA, Fallick AE (1996) A widespread positive $\delta^{13}C$ carb anomaly at around 2.33–2.06 Ga on the Fennoscandian Shield: A paradox? *Terra Nova* 8:141–157.
16 Master S, Verhagen BT, Bassot JP, Beukes NJ, Lemoine S (1993) Stable isotopic signatures of Paleoproterozoic carbonates from Guinea, Senegal, South Africa and Zimbabwe: Constraints on the timing of the *ca*. 2 Ga Lomagundi $\delta^{13}C$ excursion. *Proceedings of the International Symposium Early Proterozoic, Geochemical and Structural Constraints—Metallogeny*, ed Abdoulaye DIA (Centre International pour la Formation et les Echanges Geologiques, Dakar), pp 38–41.
17 Swart QD (1999) Carbonate rocks of the Paleoproterozoic Pretoria and Postmasburg Groups, Transvaal Supergroup. Master's thesis (Rand Afrikaans University, Johannesburg).
18 Schröder S, Bekker A, Beukes, NJ, Strauss H, van Niekerk, HS (2008) Rise in seawater sulphate concentration associated with the Paleoproterozoic positive carbon isotope excursion: evidence from sulphate evaporites in the similar to 2.2–2.1 Gyr shallow-marine Lucknow Formation, South Africa. *Terra Nova* 20:108–117.
19 Deb M, Hoefs J, Baumann A (1991) Isotopic composition of two Precambrian stratiform barite deposits from the Indian shield. *Geochim Cosmochim Acta* 55:303–308.
20 Sreenivas B, et al. (2001) Positive $\delta^{13}C$ excursion in carbonate and organic fractions from the Paleoproterozoic Aravalli Supergroup, Northwestern India. *Precambrian Res* 106:277–290.
21 Zolotarev AA, Efremov GM, Brotigam B, Ivanova TV (1989) Isotopic composition of sulfur in sulfates of Seligdar apatite deposit (Central Aldan). *Geokhimiya* 11:1656–1659.
22 Velikoslavinsky SD, et al. (2003) The U–Pb age of the Fedorov Sequence of the Aldan granulite—gneiss megacomplex, the Aldan Shield. *Dokl Earth Sci* 393:1151–1155.
23 Guliy VN, Wada H (2003) Macro- and microvariations of isotopic composition of carbon and oxygen of carbonates from the Precambrian of the Aldan Shield. *Geokhimiya* 5:482–491.